PARAMETRIC STUDY OF HALL THRUSTER OPERATION BASED ON A 2D HYBRID MODEL : INFLUENCE OF THE MAGNETIC FIELD ON THE THRUSTER PERFORMANCE AND LIFETIME

L. Garrigues[†], C. Boniface, J. Bareilles, G.J.M. Hagelaar, and J.P. Boeuf

Centre de Physique des Plasmas et Applications, Université Paul Sabatier
118 Route de Narbonne, 31062 Toulouse cedex, France

ABSTRACT

We have developed a two-dimensional hybrid model of the discharge in Hall thrusters including the near outside region between cathode and exhaust plane. The topology of the applied magnetic field is calculated with a finite element software and used as input for the discharge code. In this paper we examine the influence of the magnetic field topology on the thruster operation and properties, with emphasis on the thruster lifetime. Results show that a configuration with a zero magnetic field and a smaller region with large magnetic field tends to decrease wall erosion and low frequency current oscillations.

I. INTRODUCTION

Hall thrusters are ion thrusters where the ion beam is generated without extracting grids. The production and acceleration of ions is ensured by an external magnetic field perpendicular to the electric field. The plasma is created in a 2-3 cm channel between two concentric dielectric cylinders. The external magnetic field is radial and the applied electric field is axial. The zone of large radial magnetic field, localized in the last centimeter of the channel thruster, induces a decrease of the axial electron conductivity. The axial electric field must increase in the low electron conductivity region to maintain current continuity and this field provides ion acceleration. Electrons generated by a cathode located outside the channel enter in the channel through the exhaust plane and gain energy in the region of large electric field. The electron energy is released deeper in the channel through inelastic collisions (excitation and ionization) with the neutral atoms flowing from the anode located at the other end of the channel. The magnetic field increases the residence time of the electrons in the channel and allows collisions between electron and neutral atoms in spite of the large mean free path. Ions are not sensitive to the magnetic field and are collisionless in the channel. This highly efficient ion source offers the advantage of reducing the mass of propellant on board (and so the launch cost) compared with chemical thrusters, and is well suited to specific tasks such as satellite station keeping. At the present time, 25 satellites are equipped with Hall thrusters for satellite station keeping [1]. New missions such as deep space applications are now in consideration using 50 kW SPT [2].

[†] email : garrigues@cpat.ups-tlse.fr

The thrusters operating conditions and performance are very sensitive to the magnetic field topology. An efficient engine requires a high level of ionization and ion acceleration must be performed with minimum wall erosion. In modern SPTs, the magnetic circuit consists of two systems of magnetic coils and poles – external and internal. This magnetic system creates a quasi-radial magnetic induction in the exhaust region [3]. Magnetic screens surrounding the accelerating channel allow adjustment of the magnetic gradient in the exhaust region and reduction of the B field magnitude in the anode region [4]. The configuration of the magnetic field lines is convergent and approximately symmetric with respect to the mid surface between the channel walls. The potential drop along the B field lines is small and the equipotential contours tend to line up with the B field lines. The electric field therefore focuses the ion beam in the axial direction [5]. In this paper, we examine the effect of the magnetic field topology on the thruster regime using a two-dimensional model. This model of the discharge combines a fluid description of electrons and particle methods for atoms and ions, and includes the near field region [6], [7].

The paper is organized as follows : the model is briefly described in section II, the effect of the magnetic field topology on ion production and electric potential distribution and the consequences on the erosion are presented in part III. We then conclude in section IV.

II. DESCRIPTION OF THE MODEL

The simulation is based on a transient two-dimensional hybrid Particle-In-Cell Monte Carlo Collisions – PIC MCC model, where ion (only Xe^+) and neutral transport are described with particle methods, while the electrons are considered as a fluid. Quasineutrality is assumed and the electric field is obtained from a current continuity equation [6]. The simulation domain contains the SPT channel and the near exterior of the thruster. The discharge is simulated between the last magnetic field line totally included in the domain and the anode plane. The cathode, which is not modeled, is positioned on the last line of B field. The applied magnetic field topology is calculated using the finite element freeware package FEMM [8] (see part III.A.).

Electrons are supposed to be in Boltzmann equilibrium along the magnetic field lines. Following Morozov [5], the electric potential V is written as the sum of a potential V^* which is constant along the B field lines, and a diffusion term proportional to the electron temperature T_e :

$$V = V^* + \frac{k_B T_e}{e} \ln\left(\frac{n}{n_0}\right) \qquad (1).$$

This relation is coupled to a total current conservation equation with a given potential drop between the anode and the cathode. The electron temperature T_e is constant along the magnetic field line and calculated from the electron energy equation including a loss term due to electron-wall collisions. The plasma density n is obtained from the PIC ion transport model.

Previous works have shown that in the magnetic field configuration of a SPT, electron transport is subject to anomalous transport. Electron-atom collisions are not sufficient to account for the observed electron current and electron-wall collisions as well as field fluctuations probably play a role in the electron transport across the magnetic field lines. Due to the lack of information, “anomalous” electron transport is treated in

the model using empirical parameters. These parameters are adjusted to obtain a good match between experiments and simulations in a large range of operating conditions. An electron-wall collision frequency proportional to a constant coefficient α is added to the electron-atom collision frequency in the electron momentum transfer equation (and therefore in the expression of the electron mobility perpendicular to the B field) in the channel. In the region outside the channel, anomalous electron transport across the magnetic field is supposed to be due to Bohm diffusion, and the electron mobility in that region is written as $k/16B$, where k is an adjustable parameter (the Bohm expression of the anomalous mobility corresponds to $k \to 1$). The model results also show that electron-atom collisions are not sufficient to describe properly the electron energy loss. Energy losses due to other mechanisms (electron-wall collisions, …) must be added and described with a third parameter to obtain realistic values. Further details about theses assumptions and the numerical scheme can be found in Ref. [6].

The model has been recently improved to describe complex and realistic magnetic field configurations including structures with a zero magnetic field. The calculation domain is divided in four zones limited by the magnetic fields lines passing through the point of zero magnetic field. In each zone, the electron equations are solved separately. The solutions for the zones containing the anode and the cathode are implicitly coupled, so that a total voltage drop can be applied in the current conservation equation. The other zones are connected explicitly. In the zones where the field lines entirely close themselves on the outer or inner walls, the total current in the current conservation equation is taken to be zero.

III. RESULTS

We first describe the different magnetic configurations taken into account in the simulations. We then discuss the influence of the magnetic field topology on the thruster properties and performance. Finally, the thruster wall erosion is estimated for different magnetic field configurations.

A. Magnetic field configurations

As said in the previous section, the FEMM (Finite Elements Method Magnetic) freeware [8] has been used to calculate the magnetic field distribution for a given arrangement of the magnetic circuit. This user-friendly software solves Maxwell's equation for the magnetic vector potential in a cylindrically symmetric geometry. The details of the magnetic circuit and material properties and the current through the coils are inputs of the magnetic field code. We neglect the possible effect of the plasma current on the total magnetic induction. Different geometries of the magnetic circuit have been designed to generate different magnetic field topologies with different axial gradients of the radial magnetic field.

The magnetic field lines are plotted figure 1 for four different topologies. Note that the magnetic field in the region outside the channel and the magnetic field lens are practically the same in all configurations. In this respect, our approach is different from the study of the effect of the magnetic field variation performed by Gavryushin *et al.* [9], and Gavryushin and Kim [10]. We clearly see the presence of a region of zero magnetic field in the anode region for CASES 3 and 4. A supplementary coil, positioned behind the anode, with a negative coil current was used to create a zone of low magnetic field inside the channel [11].

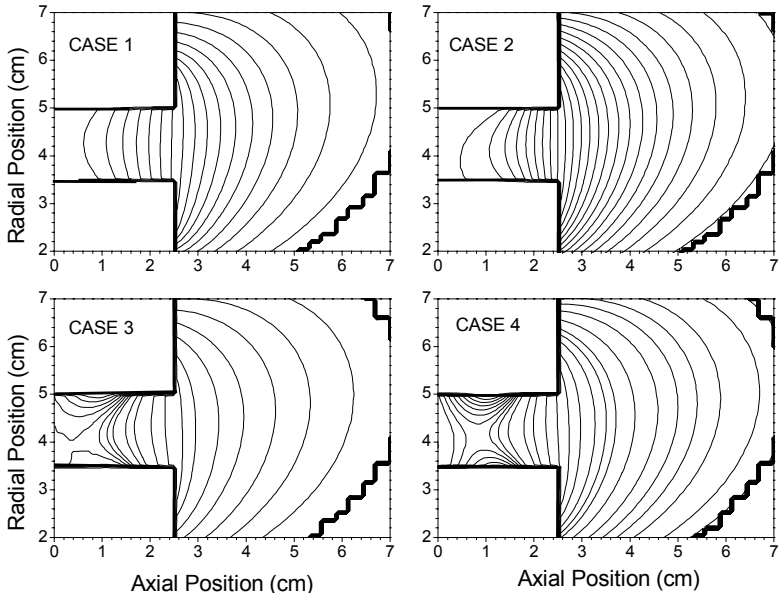

Figure 1 : SPT100 magnetic field lines calculated with FEMM for 4 different configurations of the magnetic circuit. The channel is located on the left-hand side of the plots between the radial positions 3.45 and 5 cm ; the exhaust is at an axial position of 2.5 cm.

CASE 2 corresponds to the standard configuration of the magnetic field of the SPT100-ML studied in the PIVOINE facility [12]. The calculated and measured magnetic fields (see Fig. 2) for this configuration are in good agreement (the coil current in the model has been adjusted to obtain a good match of the maximum field near the exhaust plane).

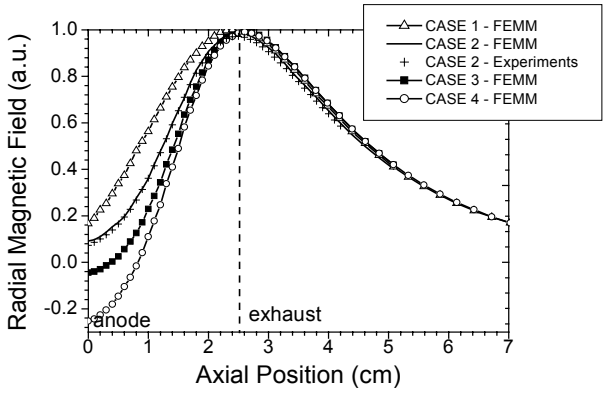

Figure 2 : Axial variations of the calculated radial magnetic field strength at the thruster channel median for different configurations. Measurements for the SPT100-ML are also plotted for CASE 2.

Variations around this configuration have been obtained by modifying the magnetic circuit. CASE 1 exhibits a larger magnetic field magnitude in the channel and a smaller gradient than CASE 2. The radial magnetic field goes through zero in the anode region and changes sign in a zone of a few millimeters in CASE 3 and 1 cm in CASE 4. The width of the region of large magnetic field is also smaller for CASES 3 and 4; this is correlated with the existence of a zero magnetic field region (the region of large magnetic field is pushed toward the exhaust when the point of zero magnetic field is shifted away from the anode).

B. Ion beam properties

The typical conditions are the following: the applied voltage is 300 V and the xenon mass flow rate is 5 mg/s. The gradient of electron temperature is set to zero on the anode while the temperature is fixed to a few eV on the cathode line. The influence of the parameters characterizing anomalous conductivity on the thruster properties has been described in the paper of Hagelaar *et al.* [7]. Comparisons between simulations and experimental results concerning the performance and the amplitude of the current oscillations [13] show that a frequency of electron-wall collisions of $\alpha \times 10^7$ s^{-1} with α=1.0 and a Bohm mobility of $k/16B$ with K=0.2 gives the best fit between experiment and simulations. We used the same values for these parameters in the present paper and for the 4 configurations of CASES 1 to 4. This seems reasonable since the magnetic field magnitude is almost the same in the region outside the channel where Bohm diffusion is important. Moreover, in the channel region near the exhaust plane, where the electron-wall collisions play an important role, the intensity of the magnetic induction is very similar in the 4 cases.

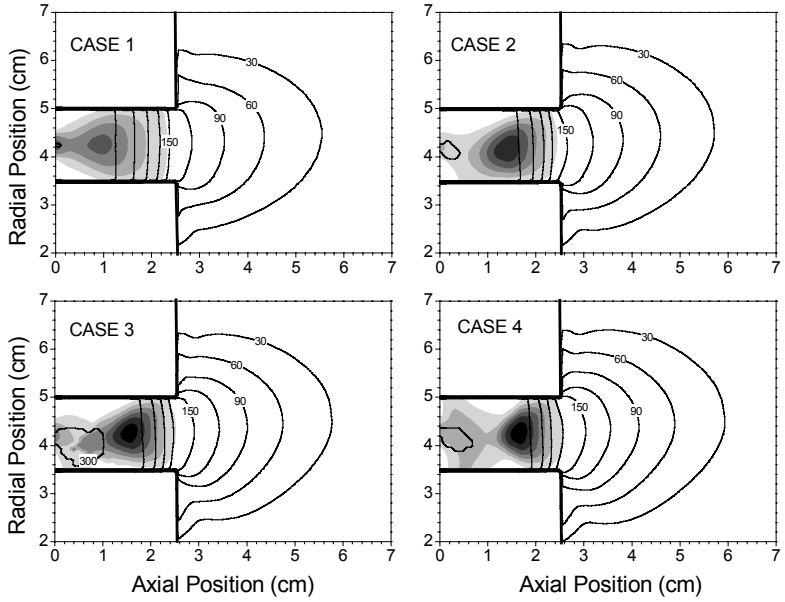

Figure 3 : Time-averaged spatial profiles of the electric potential (contours) and the ionization source term (gray scale). The contours are equally spaced with intervals of 30 V. The gray scale is linear, the intervals correspond to 10^{23} m^{-3} s^{-1}.

We have plotted in figure 3 the time-averaged spatial distributions of the ionization source term (gray scale) and the electric potential (contour lines) for CASES 1 to 4. The zone of high intensity of the magnetic field and low electron conductivity controls the spatial profile of the electric potential. Changing the width of the high magnetic field region influences the electric field distribution. The potential drop inside the channel is concentrated within few millimeters in CASE 2 and 1 centimeter in CASE 1. The low field region on the anode side extends to 2 centimeters in the cases with a zero magnetic field (CASE 3 and 4). An important part of the potential drop occurs in the region outside the channel in all cases, but the exact ratio of the potential drop inside and outside the channel is different for each case and, as expected, depends on the

magnetic field distribution. The potential drop outside the channel represents 44 % and 59 % of the applied voltage in CASES 1 and 4 respectively.

The electron energy is deposited deeper in the channel for larger widths of the region of large magnetic field as it can be deduced from the ionization source term distributions plotted in Fig. 3. A zero magnetic field topology leads to a more complex structure of the ionization rate. In the region around the location of the point of zero magnetic field the electron mobility is larger and the ionization rate decreases (see e.g., CASE 4). In the regions where the magnetic field lines are closed on the channel walls the electron mean energy and ionization source term drop. In all cases, we see a second ionization peak in front of the anode injector. The results in that region are sensitive to the boundary condition that is used for the energy equation (zero energy gradient or fixed energy). A zero energy gradient is imposed in this paper, but a fixed low electron energy would lead to a much smaller ionization rate in that region. Unfortunately, this boundary condition is rather arbitrary (although zero energy gradient seems reasonable), and there are no clear experimental data on the electron energy in this zone. Morozov and Savelyev estimate the magnitude of ionization to a relatively small value (~10 % of the maximum rate) [5]. However, we find that the influence of the boundary condition for the electron energy on the anode is not crucial for the SPT performance.

An efficient Hall thruster requires efficient ionization of the neutral flow and efficient axial acceleration of the ions (i.e. through a potential as close as possible to the total applied potential). The model results show that the total efficiency η (~50 %), the thrust T (80 mN) and the specific impulse I_{sp} - 1600 s - are almost the same for the different cases. To explain this high level of performance, we can look at the propellant utilization η_{u} (i.e. the part of xenon flux ionized) and beam energy η_E efficiency (associated to the mean energy of the ion beam compared to the potential drop). The ion production zone is clearly separated from the acceleration region (look at the position of the maximum of ion production compared to the potential fall), and ions are therefore efficiently extracted from the channel thruster, with η_E on the order of 80 %. The neutral flow is efficiently ionized since we obtain typically an efficient propellant utilization efficiency η_{u} of 90 %. We must note that in the calculations presented here, we assumed that neutrals created by ions recombination on the walls are thermalized and emitted with a temperature of 500 K. In the case of magnetic configurations with a zero B-field, the ion current striking the channel walls can reach values as high as 1 A (only 0.4 A in CASE 2). This is a consequence of fact that ions produced in the regions where the magnetic field lines are closed on the walls are lost to the walls.

C. Wall sputtering and lifetime

We included in the model the calculation of the erosion rate of the channel walls due to ion bombardment. The erosion rate (eroded thickness per unit time) is :

$$R=\frac{\Gamma_i m_w}{\rho_w}\left\langle Y(E)C(\theta)\right\rangle , \qquad (2)$$

where Γ_i is the total incident ion flux, m_w is the mean mass of the wall particles, ρ_w is the mass density of the wall material, and the triangular brackets indicate averaging over the incident ions (ion flux). The

sputtering yield Y represents the number of eroded particles per incident ion. The correction factor C accounts for the effect of the angle of incidence θ (defined with respect to the radial direction). Empirical formula for the sputtering yield Y and experimental measurements for the correction factor C are deduced from Refs. [14], [15].

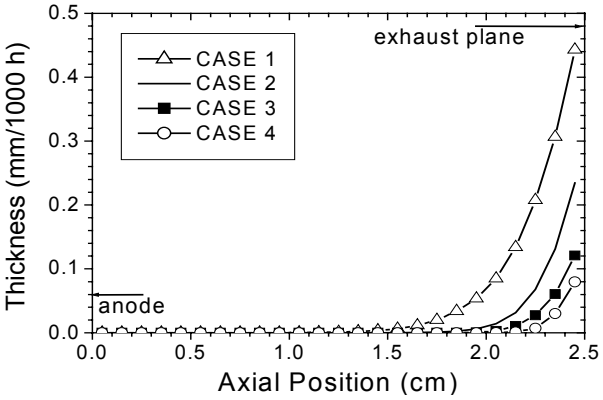

Figure 4 : Calculated erosion rate of the inner channel wall.

Figure 4 exhibits the calculated inner wall erosion rate as a function of axial position. Although the ion flux to the walls is larger deeper in the channel, the ion energy flow is much larger in the exhaust region because ion acceleration takes place in the last cm before the exhaust plane. The length of the eroded zone and the intensity of the erosion strongly depend of the configuration of the B field. A zone of 1 cm is eroded in CASE 1, only 3 mm in CASE 4. After 1000 hours of thruster operation, the maximum of material eroded in the exit plane reaches 0.5 mm for CASE 1 and only 0.08 mm for CASE 4. The length of erosion is directly connected to the positions of the source term combined with the electric potential fall. In CASE 1, the ion production and acceleration regions cover a large area of the channel, in contrast to CASE 4. A smaller electric potential drop inside the channel leads to a serious decrease in the erosion rate because of the smaller energy of the ions impacting the walls. The mean energy of ions striking the ceramics is 110 eV in CASE 1 and 80 eV in CASE 4 in the exhaust plane. Since the sputtering yield is very sensitive to the ion energy in this energy range, relatively small changes in ion energy may have dramatic consequences for the wall erosion. These results provide a quantitative confirmation of the intuitive fact that the thruster lifetime increases when a larger part of the potential drop is outside the channel. A magnetic field structure with a zero B field topology allows a reduction of the width of the large magnetic field region inside the channel and leads to good performance with improved lifetime (as observed experimentally on the PPS® 1350 [16]). However the ratio of the potential fall inside and outside the thruster also controls the beam divergence. This aspect as well as the consequences of these magnetic field configurations on low frequency oscillations (the model results show a smaller amplitude of the low frequency oscillations for CASES 3 and 4) will be further discussed in forthcoming publications.

IV. CONCLUSION

This paper is dedicated to the study of some aspects of the sensitivity of the SPT operation to the B field configuration using a two dimensional hybrid model. Different magnetic topologies with different widths of the region of large magnetic field near exhaust have been studied, keeping constant the maximum magnetic field intensity and magnetic lens. The results show that the ratio of potential drop inside and outside the channel is controlled by the magnetic field distribution and it has consequences for the thruster wall erosion and lifetime, and on the beam divergence. This is an important aspect of SPTs which is not thoroughly discussed in the literature and we think that more systematic experiments are needed to clarify this point. Systematic measurements of the part of potential inside and outside the channel (e.g. through Laser Induced Fluorescence experiments) would be very useful to confirm the effects predicted by the model. This would also help to validate the simulation results which depend on some adjustable parameters.

The transient behaviour of the thruster, not discussed in this paper, also shows that the amplitude of the low frequency current oscillations decreases when the B field configuration exhibits a zero field in the anode region (this is associated with a smaller width of the region of large radial magnetic field in our model calculations). This feature has also been observed in the ATON Hall thruster [17] where the magnetic field also goes through zero in the channel. This aspect will be discussed in future publications.

ACKNOWLEDGMENTS

This work was performed within the frame of the Groupement De Recherche CNRS/CNES/SNECMA/ONERA n°2232 "Propulsion à Plasma pour Systèmes Spatiaux". Part of this work was also directly supported by SNECMA.

REFERENCES

[1] E. Britt, and J. McVey, 38th AIAA Joint Propulsion Conference, Indianapolis, IN, 2002, paper AIAA-02-3559.

[2] D. Manzella, R.S. Jankosvsky, and R.R. Hofer, 38th AIAA Joint Propulsion Conference, Indianapolis, IN, 2002, paper AIAA-02-3676.

[3] V. Kim, Journal of Propulsion and Power **14**, 736 (1998).

[4] F. Scortecci, A. Serra, A. DiGianvito, and M. Andrenucci, 32th AIAA Joint Propulsion Conference, Lake Buena Vista, FL, 1996, paper AIAA-96-2707.

[5] A. I. Morozov and V. V. Savelyev, in : *Reviews of Plasma Physics*, Vol. 21, ed. B. B. Kadomtsev and V. D. Shafranov (Consultants Bureau, New York, 2000) pp 203-391.

[6] G. J. M. Hagelaar, J. Bareilles, L. Garrigues, and J.P. Boeuf, J. Appl. Phys. **91**, 5592 (2002).

[7] G. J. M. Hagelaar, J. Bareilles, L. Garrigues, and J.P. Boeuf, J. Appl. Phys. **93**, 67 (2003).

[8] FEMM version 3.1, by D. Meeker, (http://femm.berlios.de, 2002).

[9] V.M. Gavryushin, V. Kim, V.I. Kozlov, K.N. Kozbusky, G.A. Popov, A.V. Sorokin, M.L. Day, and T. Randolph, 30th AIAA Joint Propulsion Conference, Indianapolis, IN, 1994, paper AIAA-94-2858.

[10] V.M. Gavryushin and V. Kim, Soviet Phys. - Tech. Phys. **26**, 505 (1981).

[11] D. Valentian, A. Morozov, A. Bougrova, "Plasma Accelerator of Short Length with Closed Electron Drift", SNECMA Patent n° US5475354 (1995).

[12] V. Lago, personnal communication (2002).

[13] N. Gascon, M. Dudeck, and S. Barral, "Wall Material Effects Stationary Plasma Thruster I : Experiments", *submitted to Physics of Plasma* (2002).

[14] N. Matsunami, Y. Yamamura, Y. Itikawa, N. Itoh, Y. Kazumata, S. Miyagawa, K. Morita, R. Shimizu, and H. Tawara, Atomic Data and Nuclear Data, **31**, 1 (1984).

[15] Y. Garnier, V. Viel, J.F. Roussel, and J. Bernard, J. Vac. Sci. Technol. A **17**, 3246 (1999).

[16] M. Lyszyk, E. Klinger, O. Sécheresse, J.P. Bugeat, D. Valentian, A. Cadiou, T. Beltan, and C. Gelas, 35th AIAA Joint Propulsion Conference, Los Angeles, CA, 1999, paper AIAA-99-2278.

[17] M. Touzeau, M. Prioul, S. Roche, N. Gascon, C. Pérot, F. Darnon, S. Béchu, C. Philippe-Kadlec, L. Magne, P. Lasgorceix, D. Pagnon, A. Bouchoule, and M. Dudeck, Plasma Phys. Control. Fusion **42**, B323 (2000).